



Application of seismic stratigraphy in reservoir characterisation: a case study of the passive margin deposits of the northern Orange Basin, South Africa

Chris Adesola Samakinde^{1,2} · Jan Marinus Van Bever Donker¹ · Ray Durrheim² · Musa Manzi²

Received: 10 September 2020 / Accepted: 13 November 2020
© The Author(s) 2020

Abstract

The Barremian-Cenozoic depositional sequences in the northern Orange Basin, SW, South Africa, were investigated using the principles of seismic stratigraphy to understand the interplay of tectonics and sedimentary processes in the distribution of potential hydrocarbon reservoirs. A seismic stratigraphic workflow (seismic sequence, seismic facies and lithofacies analysis) was completed by utilising three seismic lines (L1, L2 and L3) tied to Wireline data (gamma, checkshots and sonic) in two exploration wells (A1 and A2). Seven depositional sequences were mapped followed by the creation of lithofacies log interpreted from the gamma-ray log (GR) by setting maximum GR value at 60 API for Sandstone, 60–100 API for Siltstone and above 100 API for Shale. Six seismic facies units are recognised based on internal geometry and configurations of the seismic reflectors; Tangential-Oblique (SF1), Hummocky (SF2), Wavy-Parallel (SF3), Chaotic (SF4), Sub-parallel/parallel (SF5) and Divergent (SF6). SF4 is dominant within the Barremian-Aptian sequence and expressed in an incised valley fill, suggesting mass transport deposition accompanied by strong hydrodynamic conditions. Evidence of sedimentary basins progradation is seen within the Late-Albian-Turonian sequences, because of the occurrences of SF2, SF6 and SF 4 facies. SF5 facies is prominent in the Maastrichtian/Campanian sequence, indicating that the deposition of sediments may have been accompanied by uniform margin subsidence after the Late-Cretaceous uplift of the Africa margin. The occurrence of SF1 and SF4 facies within the Cenozoic sequence indicates terrigenous pro-deltaic deposits and mass transport deposits, respectively. Further results from seismic-lithofacies modelling reveal that sand deposits of Barremian-Aptian (SF4 facies unit) and Albian sequences (SF2 and SF6 facies units) are potential stratigraphic reservoirs in this part of the basin.

Keywords Facies modelling · Orange Basin · Seismic facies

Introduction

As passive margin terrains are structurally less complex than active tectonic regimes, they preserve sedimentary records which can easily be investigated. The application of seismic stratigraphic concepts in the investigation of the sedimentary successions in passive margin settings is critical to the understanding of the palaeo-environments and the geodynamic evolution of sedimentary basins, viz the structural

styles and depositional systems. Consequently, potential hydrocarbon reservoirs can be explored for drilling campaigns and sampling of cores for reservoir quality analysis and prediction.

The modern passive margins generally have a mean age of 104 Ma and are a host to 35% of global giant oil discoveries (Bradley 2008; Mann et al. 2003) and often exhibit similarity in structural styles and sedimentary patterns particularly in conjugate basins. Two of the recent hydrocarbon discoveries in conjugate passive margin settings were from the Albian-age sandstone reservoirs of the southern Orange Basin, South Africa (Petroleum Agency SA report 2010), and in Brazil, from the Barremian-Aptian syn-rift non-marine microbial carbonates of the Santos Basin (Scotchman et al. 2010). In both cases, the reservoir quality is controlled by a multi-phase diagenesis (Levell et al. 2009; Fadipe et al.

✉ Chris Adesola Samakinde
chrissamakinde@gmail.com

¹ Department of Earth Sciences, University of the Western Cape, Capetown, South Africa

² School of Geosciences, University of Witwatersrand, Johannesburg, South Africa

2011), thereby posing a challenge for predicting reservoir quality distribution.

Whilst exploration continues within the syn-rift pre-salt sequences of the Santos Basin (Scotchman et al. 2010), further exploration is essential in northern Orange Basin for the delineation of potential reservoirs for a drilling programme.

The Orange Basin situated on the passive western margin of South Africa (Fig. 1), preserves a remarkably complete sedimentary record because the depositional system was seldom affected by tectonic forces, apart from gravity flow (Rebesco et al. 2017; de Vera et al. 2010). Previous studies of the southern Orange Basin (Samakinde et al. 2016; Fadipe et al. 2011) found that potential clastic reservoirs are poorly developed due to the severe precipitation of diagenetic cements that reduced the porosity and permeability. This is evident with the Ibhubesi tight gas discovery in the southern part of the basin (Petroleum Agency SA Report 2006).

Here we investigate the distribution of potential stratigraphic reservoirs in the northern part of the Basin (Fig. 1) by applying the principles of seismic stratigraphy (Mitchum et al. 1977; Vail 1987; Cross and Lessenger 1988; Catuneanu 2006). The objectives of this study are: (1) the analysis

and interpretation of seismic sequences and facies within a chronological framework to infer sedimentary environments of the deposits. (2) The integration of seismic and lithofacies analysis to investigate tectono-sedimentary evolution and the implication for the distribution of potential hydrocarbon reservoirs within the study area. We use two 2D seismic lines (L1, L2) to tie exploration well A1; geophysical logs from two exploration wells A1 and A2 (see Table 1); and an inline (L3) extracted from a 3D reflection survey patch to tie well A2 (Fig. 1).

The workflow begins with mis-tie analysis of the seismic lines to match their vintages followed by a tie of the seismic lines with the wells utilising sonic log, checkshots and formation tops to generate a synthetic seismogram. The formation top markers were used to delineate the chronology of depositional sequences from Barremian-Aptian to Cenozoic age. This is followed by seismic sequence analyses which involves the mapping of reflection terminations against major discordant surfaces (onlap, downlap, toplap and truncation). Next, the seismic facies between bounding unconformities are characterised based on the amplitude, continuity and character of reflections of the various

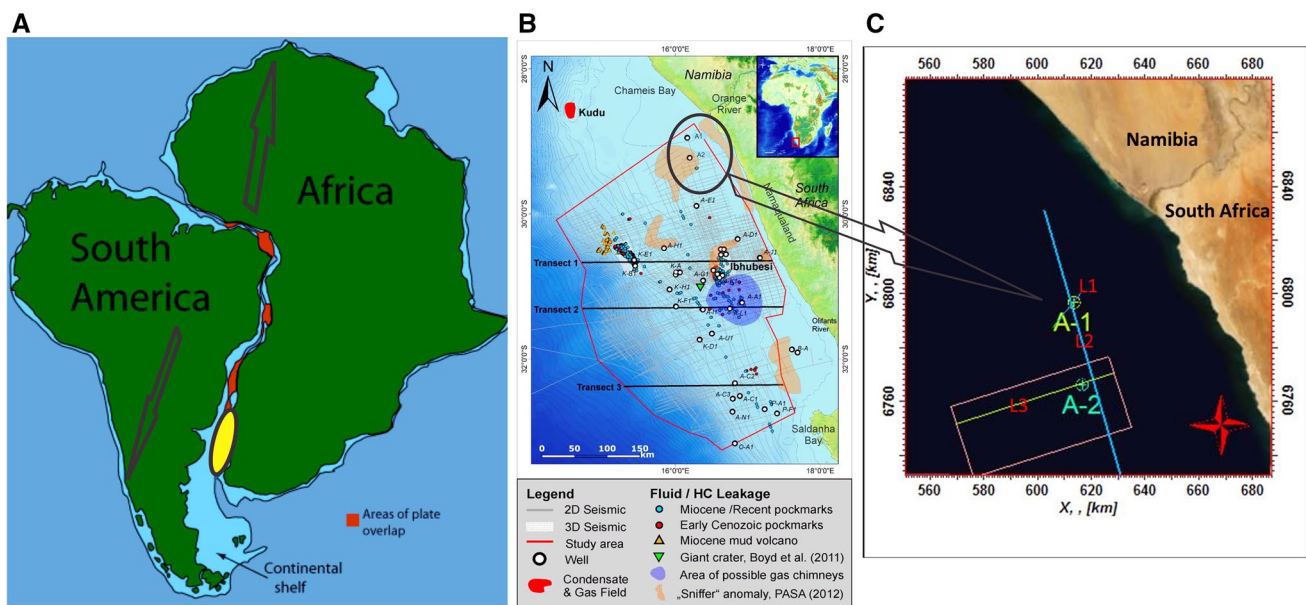


Fig. 1 a–c (a) Location map of the study area showing the South American and African plates as part of West Gondwana, and the position of the Orange Basin (shaded yellow circle) in the late Jurassic (Figure modified from Lutgens and Tarbuck, 2014). (b) Map of

the Orange Basin showing the wells, seismic data and geological features. The study area is in the black circle. Figure modified from (c) A map showing wells A1 and A2, the 2D seismic lines (L1, L2) and a 3D inline (L3) used for this study Hartwig (2014).

Table 1 Position, water depth and total depth of wells used for this study

Wells	Longitude	Latitude	Kelly bushing (m)	Water depth (m)	Total depth (m)
A2	16° 11' 58.4"E	29° 11' 27.7"S	25	166	4003
A1	16° 09' 56.37"E	28° 56' 54.59"S	25	180	4605

depositional sequences (e.g. Sangree and Widmier 1979; Badley 1985). Finally, these analyses are aided by the interpretation of gamma-ray log signatures, in addition to lithology cross section, to understand the sedimentary distribution and palaeo-environments of the deposits encountered in the study area.

Structural evolution and geology of the Orange Basin

The South American and African plates were part of West Gondwana until the late Jurassic (Fig. 1), when a narrow western margin of South Africa was formed when regional rifting, accompanied by volcanism caused the drifting apart of the African and South American plates (Gladchenko et al. 1997, 1998 and Bauer et al. 2000). The Etendeka Basalt, found in the northern part of the Orange Basin, is evidence of this volcanism (de Vera et al. 2010). The Orange Basin, characterised by graben structures that trend sub-parallel to the coastline (Jikelo 1999), is the major repository for a mix of continental and volcanic sediments (Fatti et al. 1994) supplied by the Orange, Olifants and Berg rivers (Brown et al. 1996).

Sedimentation in the proto-Orange Basin probably began shortly after the onset of rifting in the Kimmeridgian stage of the Late Jurassic epoch (154–152 Ma) and comprises

alluvial and deltaic sediments (Broad et al. 2007). The main drift phase began in the Mid-Cretaceous epoch (around 112 Ma) and is marked by a major unconformity marked SQ5 in this study (Fig. 2). The Olifants river supplied sediments to the southern Orange Basin from 117.5 to 103 Ma, while regional drowning was initiated around 110 Ma (Fig. 2). The Orange River supplied sand-rich sediments to the northern part of the Orange Basin around 103 Ma as a result of the reworking of the delta front and marine storm channel bars, as well as wave action effects (Brown et al. 1996). The sands are generally well-sorted, ranging in grain size from very fine to medium-grained. At least 30 third-order post-drift sequences were deposited during the Cretaceous, with a total thickness of some 8 km in the depocentre (Brown et al. 1996). The sediments deposited in the Cenozoic epoch are mostly calcareous oozes and chemical sediments such as banded iron formation in a thick wedge characteristically deformed due to sediment loading and slope instability (Petroleum Agency SA, 2006).

Methodology and interpretative methods

Datasets and seismic-well-tie

Two 2D seismic lines (L1, L2) and an inline (L3) shot in the NE–SW, NW–SE and ESE–WSW directions, respectively,

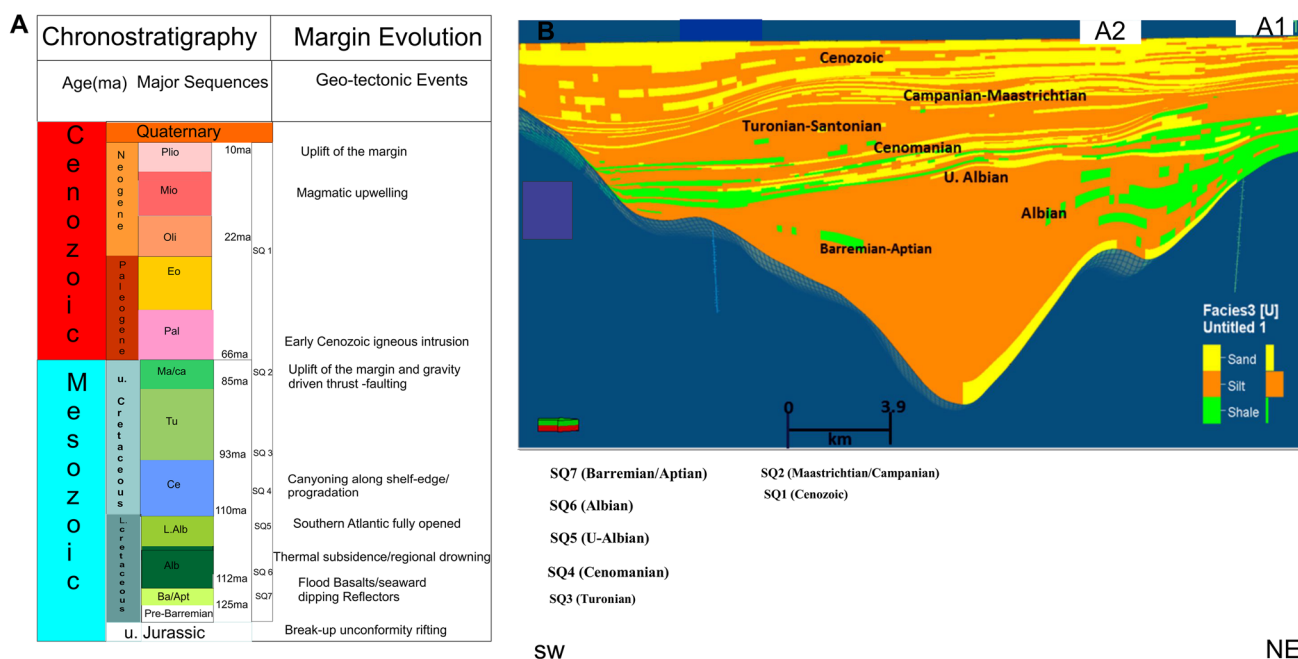


Fig. 2 a–b (a) The localised chronostratigraphy of the Orange Basin (within study area) detailing the major sequences mapped (SQ7–SQ1) for this study and the events that characterised the evolution of the Western Margin. The Santonian and Coniacian Sequences are not

mapped as they are not deposited within the study area. (b) A geological cross section covering the study area showing distribution of lithologies of different ages marked from SQ7 (Barremian–Aptian) to Cenozoic (SQ1) and wells A1 and A2 used for the study

were used in this study (Fig. 1). In addition, a suite of wire-line logs (gamma ray, sonic and density) was interpreted on the Petrel 2015 workstation. These logs were spliced to obtain a continuous run in the two wells (A1 and A2), and seismic horizons were mapped from the well positions after an initial seismic well-tie had been performed (Fig. 3). This was done by calibrating sonic, density, check shots and formation tops data to establish a time depth relationship between wells and seismic data and to generate a velocity log. This was followed by the generation of a synthetic seismogram using the density, velocity log, Ricker zero-phase wavelet and the Society of Exploration Geophysicist (SEG) normal polarity with a frequency range between 100 and 125 Hz (Fig. 3). Finally, bulk shifting was done for an

amplitude match between the seismic signatures and the synthetic seismogram.

The seismic–well tie shows the depth function Z (m) (Fig. 3). These depths (Z) represent seismic horizons and the formation tops (unconformities) mapped within the Orange Basin chronological framework which are marked from SQ7-SQ1 for the current study (Fig. 2).

Seismic stratigraphy

The interpretative methods of Vail 1987, Sangree and Widmier 1979 and Badley (1985) (Table 2) were applied in this study. After seismic sequences were classified as genetically related stratigraphic units, erosional surfaces within

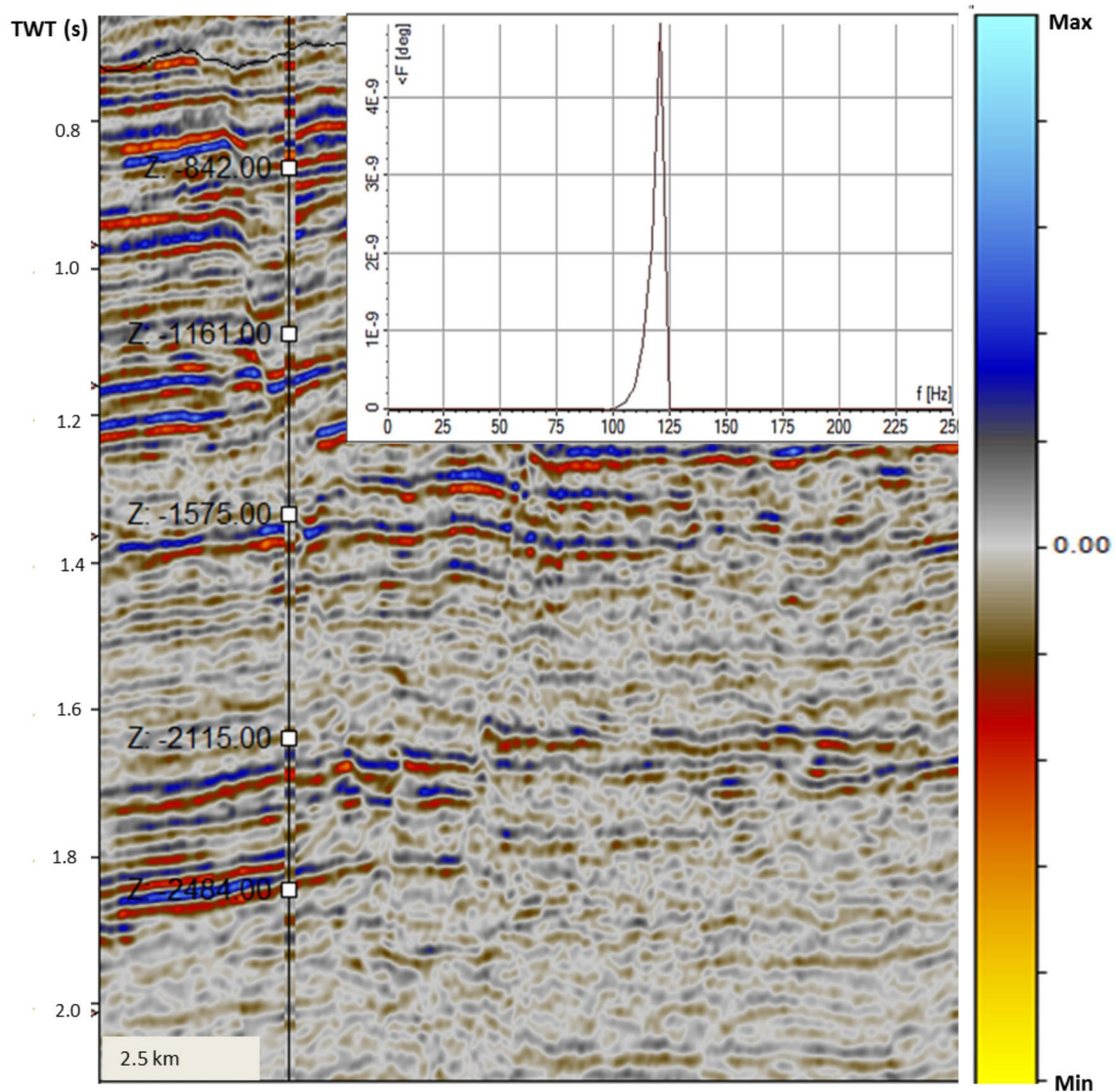


Fig. 3 The synthetic log generated from well A2 tied to the seismic line L3 with depth function Z (m) to align formation tops with their actual positions for mapping each sequence (SQ1-SQ7). Inset is the

Ricker wavelet displaying the amplitude and the frequency of the seismic lines used for this study

Table 2 Summary of different seismic facies (Badley 1985)

Seismic facies	Reflection configuration	Reflection continuity	Reflection amplitude and frequency	Bounding relationship	Depositional environment interpretation	Example (Vertical scale bars represent 100 ms)
1 Parallel continuous high amplitudes	Parallel	Continuous	High amplitude and low frequency	Continuous and draping underlying topography	Pelagic or hemipelagic	
2 Semiparallel continuous high amplitudes	Semiparallel	Continuous to semicontinuous	High amplitude and high frequency	Restricted to the top of the regional anticline	Debris flows or hyperconcentrated density flows or turbidites	
3 Mounded discontinuous low amplitudes	Contorted to mound-shaped	Discontinuous	Low amplitude and high frequency	Onlap, downlap, toplap, and truncation	Debris flows or (hyper) concentrated density flows	
4 Blocky semicontinuous high amplitudes	Oblique	Semicontinuous	High amplitude and high frequency	Separated by linear vertical to oblique surfaces	Lower slope and slumps or large lithified collapse blocks	
5 Oblique semicontinuous high amplitudes	Oblique	Semicontinuous	High amplitudes	Thinning out toward the platform	Upper slope	
6 Chaotic amplitudes	Chaotic	Discontinuous	Low amplitude	Grading vertically to facies 7 and laterally to facies 5	Platform interior	
7 Mounded semicontinuous high amplitudes	Contorted to mound-shaped	Semicontinuous	High amplitude and low frequency	Numerous diffraction hyperbolas	Karstified platform top	

these depositional sequences were first mapped followed by seismic facies characterization. This involved analysing the geometry and configurations of the seismic reflectors, including their continuity and amplitude coupled with the identification of reflection patterns, as described by Badley (1985). The interpretation made on each depositional sequence was calibrated at the well positions (A1 and A2) with interpretations made from the gamma-ray log signatures (Figs. 5, 6, 7, 8, 9, 10, 11). This was done in order to compare interpretations of depositional environments made from both the seismic-and well data. The seismic facies discrimination criteria used were based on the reflection configuration, internal geometry and amplitude of the reflectors as documented by Badley (1985). Finally, six seismic facies units are recognised based on clinoform reflection configurations and geometry, viz. Tangential-Oblique (SF1), Hummocky (SF2), Wavy-Parallel (SF3), Chaotic (SF4), Subparallel/parallel (SF5) and Divergent (SF6).

Lithofacies analysis

In this study, due to a lack of available cores, a lithology log interpreted from the gamma-ray (GR) log was integrated with seismic facies analyses to infer the palaeo-environments within the study area. The lithology log was created using a value discriminant where GR values less than 60 API are classified as sandstone, GR values between 60 and 100 API

are classified as siltstone, while GR values greater 100 API are classified as shale. A lithology cross section was constructed from an upscaled lithology by adopting a sequential indicator simulator process to simulate a discrete property (facies). The simulation uses a kriging indicator, which is determined by taking an average frequency and variation of the discrete spatial continuity. The simulator gives consideration to parameters such as anisotropy and heterogeneity and consequently reduces the uncertainty associated with using sparse data during the simulation process.

Results

Seismic sequence analyses

The seismic lines used for the analysis of the depositional sequences are L1 (North), L2 (Central) and an inline L3 (South) (Fig. 4). These depositional sequences are divided into packages within a chronological framework (Fig. 2) separated by regional unconformities and are coded from SQ1–SQ7, where SQ 7 (Barremian) is the oldest sequence and SQ1 (Cenozoic) the youngest sequence mapped (Fig. 4). There are onlapping clinoforms observed within the Barremian-Aptian sequence (SQ7) which are consistently present across the study area, and this represents the on-lapping of the SQ7 sequence against the surface of a down-dipping

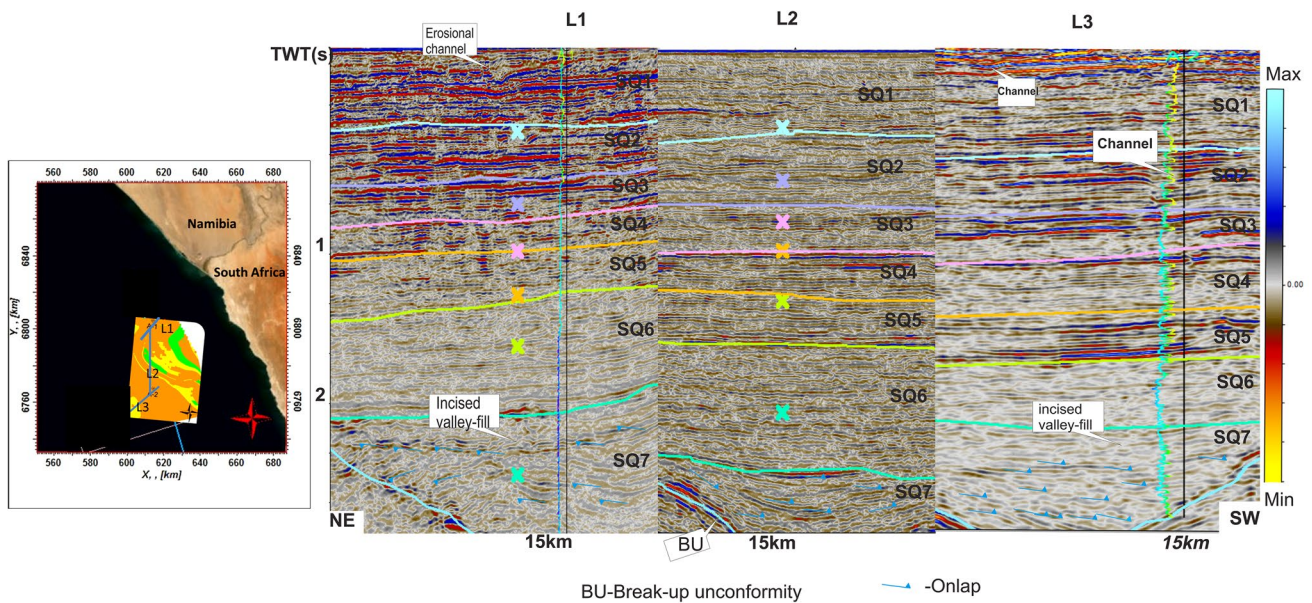


Fig. 4 a–c The three seismic profiles; L1(A84-007), L2 (SA92-106) and L3(2370) in TWT (s) and the respective gamma-ray logs of the control wells (A1 and A2) in the Northern and Southern section. The Central part has no well tied to the Seismic line L2. The blue arrows

on the seismic lines indicate the termination of SQ7 clinoforms against a down-dipping surface (onlap). SQ1—Cenozoic; SQ2—Maastrichtian/Campanian; SQ3—Turonian; SQ4—Cenomanian; SQ5—Upper Albian; SQ6—Albian; SQ7—Barremian-Aptian

basement (Fig. 4). This sequence appears to have been deposited as an incised-valley fill in the study area. There is evidence of a major erosional channel on seismic lines L1 and L2 within the SQ1 sequence (Fig. 4). A channel is also mapped within the SQ2 sequence close to well A2 (Fig. 4). There is no exploration well drilled in the central part of the seismic profile (L2); hence, there is no available well log to compare and validate the analysis of the seismic sequence.

Seismic and lithofacies analyses

SQ7 (Barremian-Aptian)

The SQ7 (Barremian-Aptian) sequence shows low-amplitude, chaotic facies (SF4) in a v-shaped Incised-Valley Fill (IVF) in the northern part, moderate-amplitude and hummocky reflection configurations (SF2) in the central part, while the southern part equally exhibits a chaotic Incised-Valley Fill (SF4) (Fig. 5a–c). The TWT ranges between 2.2 and 2.8 s for the entire sequence within the study area. The SF4 suggests dominance of a high-energy environment accompanied by mass transport of sediments, while the SF2 represents strata forming as small lobes in a pro-deltaic environments. The calibrated gamma-ray log for the sequence in well A1 (northern part) shows a switch from progradation to retrogradation at around 4000 m depth in the north, and at 3300 m depth, the log signature indicates an incised channel fill deposit coupled with the serration of

the prograding pattern of the log (Fig. 5a). In addition, the calibrated gamma-ray log in well A2 (southern part) shows an initial fining upward sequence between 3840 and 3900 m followed by an intercalation of silt and sandstone deposits (Fig. 5c).

SQ6 (Albian)

The SQ6 Albian sequence exhibits low amplitude, sub-parallel clinoforms (SF5) in the northern part (Fig. 6a). In the central section, the facies is dominantly of high amplitude and exhibits divergent continuous reflectors (SF6), underlain by hummocky (SF2) reflection configurations around 2.4 s TWT (Fig. 6b). The southern part displays low-amplitude, chaotic clinoforms (SF4) (Fig. 6c). The SF5 facies is interpreted as a deposition on a uniformly subsiding shelf margin, SF6 facies is suggested to have been deposited due to variation in the rate of sediment supply, SF2 as strata forming as small lobes in a pro-deltaic environments, and SF4 facies is suggested to have been deposited in a high-energy depositional environment which led to the chaotic facies (SF4).

In the northern section, the gamma-ray log signature shows a serrated fining-upward sequence with shale/silt intercalations dominant around 2700 and 2800 m, and this unit fines upward into a massive shale deposit between 2100 and 2500 m in the northern part (Fig. 6a). The gamma-ray log within this unit shows serration, and an initial fining-upward sequence which switched into an aggradational pattern with shale and silt intercalation around 2800 m in the

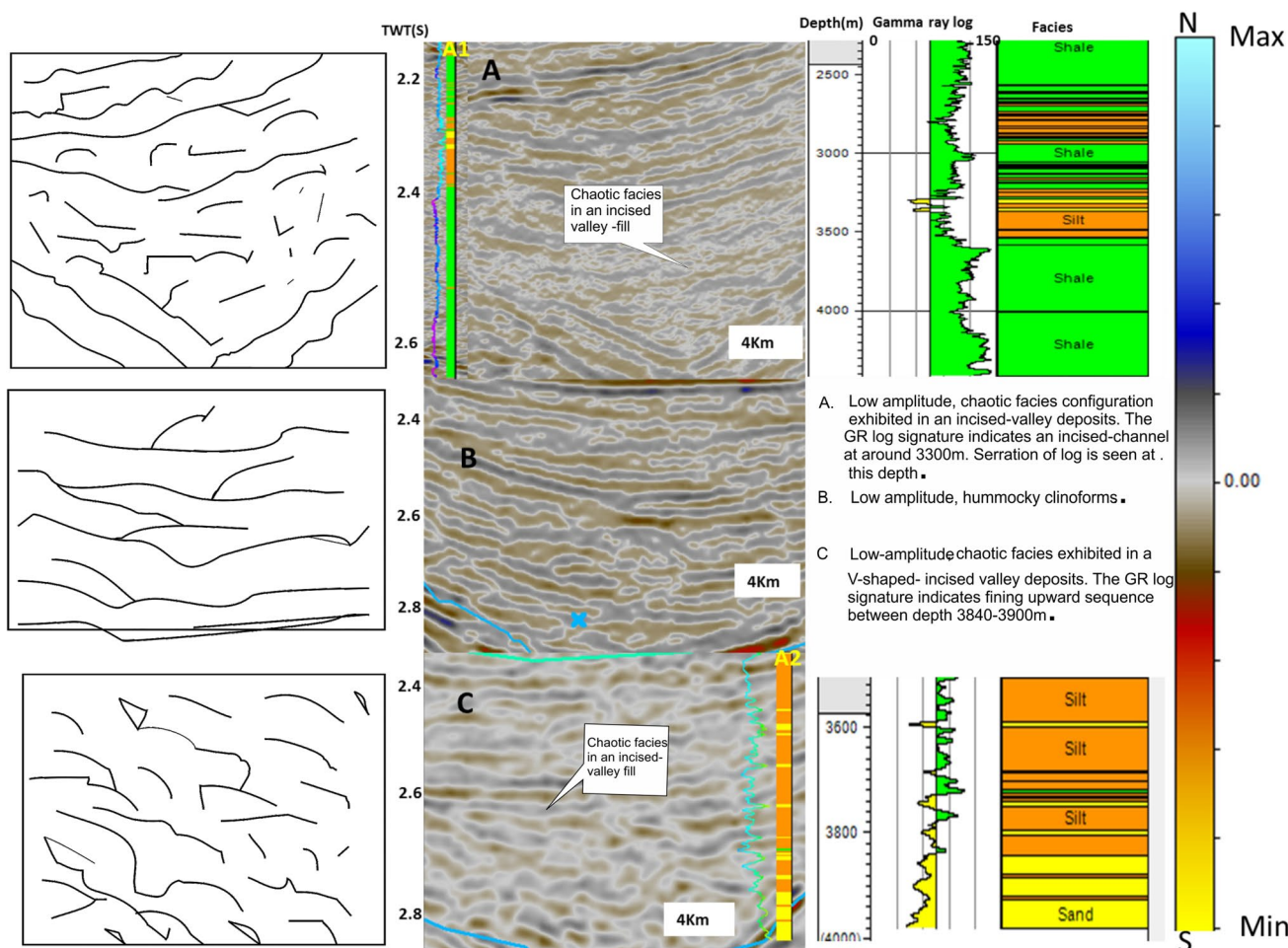


Fig. 5 a–c Barremian-Aptian seismic facies configurations and calibrated gamma-ray logs with the lithology interpretations at well positions along the N-S profile. A (North), B (Central) and C (South). On the left are the conceptual representations of the seismic facies. The

horizontal length of each seismic section is 4Km. Note seismic facies mapped within this sequence are Chaotic (SF4) and Hummocky (SF2)

southern part (Fig. 6c). Serration of the GR log as observed in the northern and southern part may be attributed to storms and waves dominance which accompanied the deposition of the sediments on the shelf. The TWT for the entire sequence ranges between 1.6 and 2.5 s (N–S). In summary, the seismic facies encountered within this sequence are sub-parallel (SF5), divergent (SF6), hummocky (SF2) and chaotic (SF4) clinoforms.

SQ5 (Upper-Albian)

The seismic facies of the late-Albian sequence is characterized by low-amplitude, hummocky reflection configurations (SF2) in the northern part (Fig. 7a) which changes into high amplitude and divergent clinoforms (SF6) in the central part (Fig. 7b). The southern part exhibits low to moderate-amplitude chaotic patterns (SF4) (Fig. 7c).

Based on these reflection configurations, the depositional environment of SF2 is suggested to be pro-deltaic with sediments forming in small lobes. The SF6 reflection configurations are seen climbing down, a likely indication of variation in the rate of sediment deposition, while SF4 may have occurred in a highly variable energy environment causing the chaotic configurations observed here (SF4). In summary, the seismic facies dominant in this sequence are hummocky (SF2), divergent (SF6) and chaotic (SF4) reflection configurations.

The GR log displays a blocky aggradational pattern in the northern part typical of massive shale and silt deposits evident between 1600 and 2000 m (Fig. 7a) and an aggradational intercalated sand and silt sequence in the South (Fig. 7c). The TWT for the entire sequence ranges between 1.3 and 1.8 s (Fig. 7a–c).

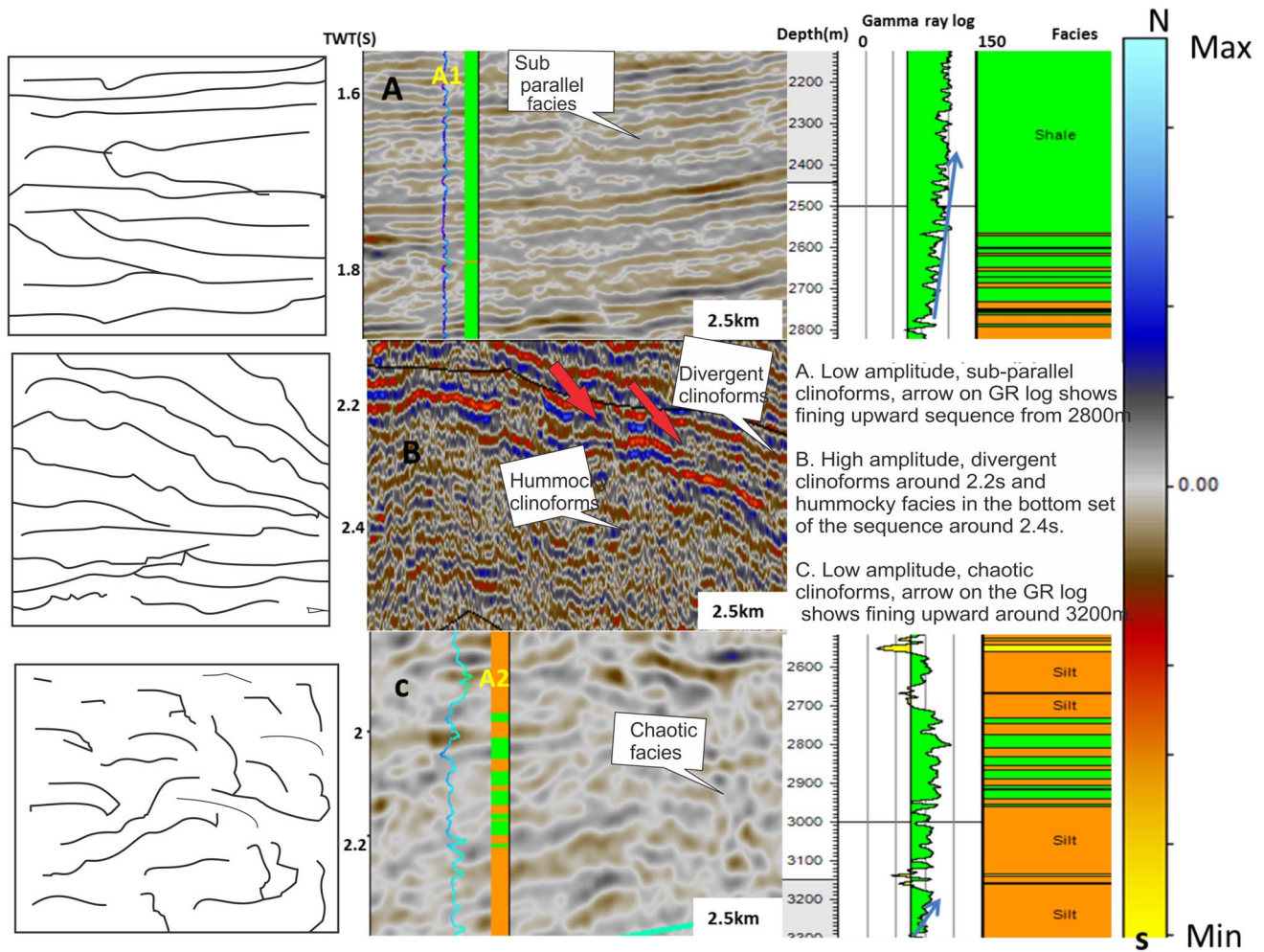


Fig. 6 a–c Albian Seismic facies configurations and calibrated gamma-ray log with the lithology interpretations at well positions along the N–S profile. A (North), B (Central) and C (South). On the left are the conceptual representations of the seismic facies. The hori-

zontal length of each seismic section is 2.5Km. Note seismic facies mapped in this sequence are Hummocky (SF2), Sub-parallel/Parallel (SF5) and Chaotic (SF4)

SQ4 (Cenomanian)

The Cenomanian (SQ4) sequence displays low–medium-amplitude and sub-parallel clinoforms (SF5) in the northern, central and southern part of the study area (Fig. 8a–c), suggestive of a uniformly subsiding shelf, coupled with uniform rates of deposition. The calibrated gamma-ray log displays a ‘saw teeth’-like serration, which indicates the influence of waves and storms, a phenomenon common on the shelf (Fig. 8a). The southern part shows an initial fining upward sequence around 1500 m and culminates into a likely delta front distributary channel sands at about 1350 m (Fig. 8c), the evidence of which is observed within the SQ2 sequence on the seismic section (see Fig. 4). The TWT for the entire sequence ranges between 1.1 and 1.6 s (N–S).

SQ3 (Turonian)

The seismic facies unit of the northern section of Turonian sequence comprises of high-amplitude parallel/sub-parallel (SF5) reflection configurations (Fig. 9a). Low-amplitude hummocky (SF2) configurations are observed in the central part (Fig. 9b), while the facies unit in the southern part indicates moderate–high-amplitude chaotic reflection (SF4) configurations (Fig. 9c). SF5 is often associated with uniformity in sediment deposition on a stable shelf, which could grade into a delta plain basinward, while SF2 indicates the building of deltaic lobes into relatively shallow water in a pro-deltaic environment. The chaotic reflection (SF4) configuration often represents a depositional system of mud-rich coarse-grained turbidite channels accompanied by variability in the energy of the depositional environment.

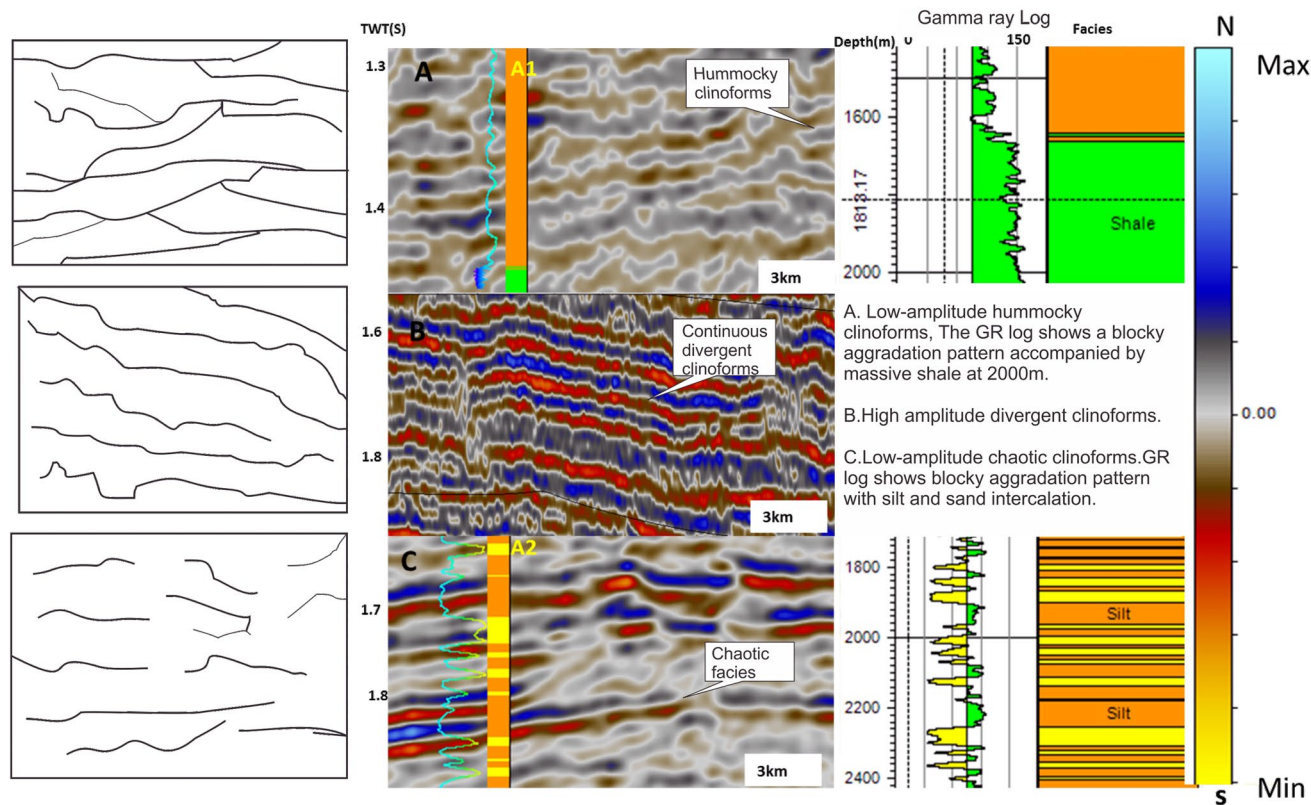


Fig. 7 a–c Late-Albian seismic facies configurations and calibrated gamma-ray log with the lithology interpretations at well positions along the N–S profile. A (North), B (Central) and C (South). On the left are the conceptual representations of the seismic facies. Horizontal

length of each seismic section is 3 km each. Note seismic facies mapped in this sequence are Hummocky (SF2), Divergent (SF6) and Chaotic (SF4)

The gamma-ray log interpretation suggests that sand deposits seen at 850 m may be of deltaic origin (Fig. 9a). A similar interpretation was made from the gamma-ray log in the southern part which suggests that the sand deposit may be of turbiditic origin, evidenced by the fining upward sequence of sand into silt around a depth of 900 m (Fig. 9c). The TWT for the entire sequence ranges between 0.9 and 1.4 s (N–S). In summary, there are three seismic facies units within this sequence (Sub-parallel/parallel SF5, Hummocky SF2 and Chaotic SF4).

SQ2 (Maastrichtian/Campanian)

The seismic facies of the Maastrichtian/Campanian sequence unit exhibits sub-parallel (SF5) low–medium–high-amplitude clinoform configurations in the northern, central and southern parts, respectively (Fig. 10a–c). This suggests shelfal deposition and an indication of sediments deposited on a uniformly subsiding shelf. The gamma-ray log at the well position shows two prograding coarsening upward sandstone depositional sequences intercalated with silt between 480 and 600 m. This is followed by an aggrading pattern signature and serration of the log, most obvious around the

massive siltstone deposit at depth of 400 m (Fig. 10a). A fining-upward sequence as seen on the gamma-ray log in the South indicates back-stepping of sediment deposition around 600 m (Fig. 10c). The TWT for the entire sequence ranges between 0.6 and 1.1 s (N–S).

SQ1 (Cenozoic)

The SQ1 Cenozoic clinoforms in the northern part of the study area show moderately high amplitude and tangential-oblique prograding reflection configurations (SF1) (Fig. 11a), while the central part of the sequence exhibits seismic reflections which are generally low-amplitude, hummocky reflection configurations (SF2) (Fig. 11b). The southern part of the study area shows low-amplitude chaotic (SF4) configurations in the lower part, and high-amplitude, mounded strong wavy-parallel (SF3) configurations in the upper part (Fig. 11c). The SF1 is interpreted as shelf margin shoreface (sand rich) deltaic deposits in the North. The SF2 configurations in the Central part could represent strata forming as small clinoform lobes in a pro-deltaic environment, while the SF3 represents shelfal deposits accompanied by strong wave action. The calibration of these observations

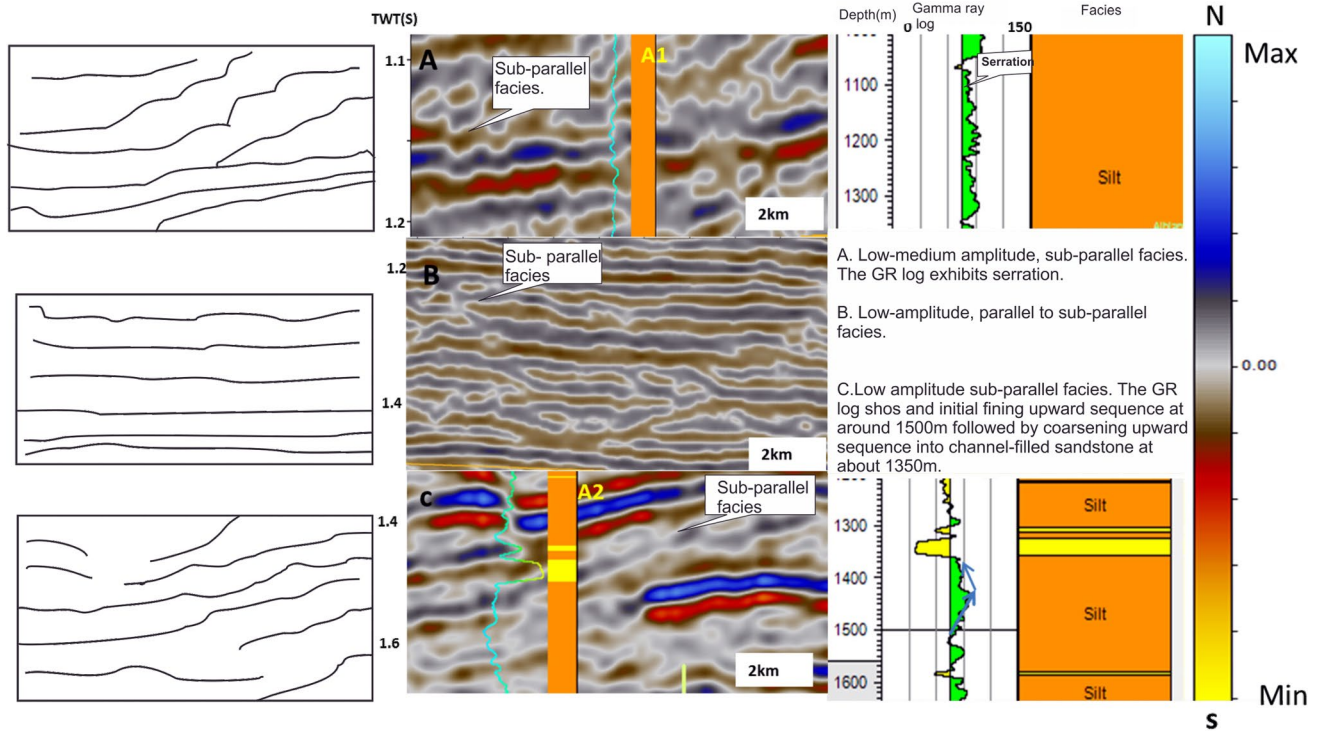


Fig. 8 a–c The Cenomanian seismic facies configurations and calibrated gamma-ray log with the lithology interpretations at well positions along the N–S profile. A (North), B (Central) and C (South).

On the left are the conceptual representations of the seismic facies. Horizontal length of each seismic section is 2 km. Note seismic facies mapped in this sequence are Sub-parallel (SF5)

with the gamma-ray log signatures indicates a coarsening-upward prograding sand deposit suggestive of pro-delta shoreface sands in the North (Fig. 11a). An aggrading gamma-ray log signature is interpreted in the South, likely due to the stacking up of sand deposits. This is coupled with the serration of the log as observed around 400 m, indicating a storm and wave-dominated shelf environment (Fig. 11c). The TWT for the entire sequence ranges between 0.2 and 0.7 s (N–S).

Discussion

Seismic sequences

The post-rift evolution of the Orange Basin has been well studied with the sedimentary evolution classified into three main stages in the Lower Cretaceous, Upper Cretaceous and the Cenozoic eras (Emery et al. 1975; Gerrard and Smith 1982 and Brown et al. 1996). In this study, seven depositional sequences are classified as above: the Lower Cretaceous (SQ7, SQ6, SQ5), Upper Cretaceous (SQ4, SQ3, SQ2) and SQ1 in the Cenozoic. The analyses of the seven seismic sequences reveal the presence of channels

within the Cenozoic (SQ1) and Maastrichtian/ Campanian sequences (SQ2) (Fig. 4). The channels within the SQ1 are likely to be palaeo-channels of the Orange river because the discharge outlet is suggested to have switched northwards to the current study area due to a topographic barrier to the South during the Cenozoic era (Dingle and Hendley 1984). A channel-like feature identified within the SQ2 sequence close to well A2 is validated by the interpretation of the gamma-ray log which shows a fining upward sequence around 700 m (Fig. 10c), an indication of a fluvial channel. The onlap sequences localised to the Barremian-Aptian sequence in the northern and southern part of the study area (Fig. 4) may have been a response to the coupling of high sedimentation rates and high thermal subsidence. The combination of high sedimentation rates and high thermal subsidence possibly led to mass movement of sediments leading to the formation of incised valleys in which the onlapping sequences occurred. This period is marked by the formation of ‘saucer-shaped depocentres’ in which sedimentation occurred (Kuhlmann et al 2010). Saucer-shaped depocentres as referred to by Kuhlmann et al. (2010) are suggested to be an incised valley accompanied by strong hydrodynamic conditions.

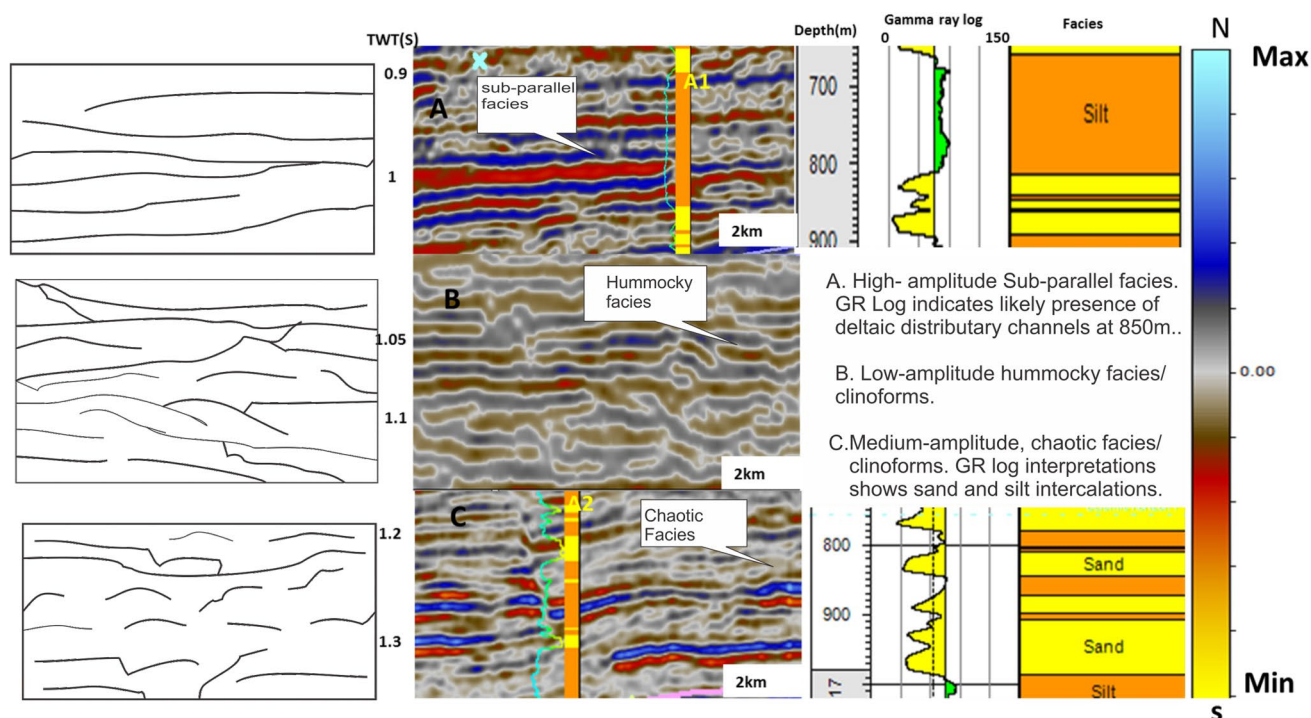


Fig. 9 a–c Turonian seismic facies configurations and calibrated gamma-ray log with the lithology interpretations at well positions along the N-S profile. A (North), B (Central) and C (South). On the left are the conceptual representations of the seismic facies. Hori-

zontal length of each seismic section is 2 km. Note seismic facies mapped in this sequence are Sub-parallel/Parallel (SF5), Hummocky (SF2) and Chaotic (SF4)

Seismic and lithofacies

The basin evolution during the Barremian-Aptian times was characterised by high run-off from the hinterlands which resulted in topographic discontinuities in addition to high thermal subsidence (Kuhlmann 2010). The high run-off effect could possibly have led to the deposition of sedimentary facies characterised by the chaotic pattern (SF4) of the V-shaped incised valley reflectors seen within the Barremian-Aptian sequence (Fig. 5a–c). Deposition of incised valley fill is often influenced by strong hydrodynamic conditions, which could transport massive sedimentary units into the basin (Zhu et al. 2012). The incised-channel fill is equally observed on the gamma-ray log signature in the northern section of the sequence at around 3300 m (Fig. 5a). This indicates a thin sandstone deposit with a very low GR value suggesting a coarse-grained sand deposit at a depth of around 3350 m in the northern part, followed by the deposition of massive shale deposits at around 3000 m (Fig. 5a). The shale deposits are linked to the anoxicity that prevailed during the Aptian marine transgression (Jungslager 1999). The seismic facies mapped in the SQ7 sequence are SF4 in the North and South, while SF2 is observed in the Central part of this sequence.

An evidence of a uniformly subsiding continental shelf during the Albian period is seen in the northern part of our study area because the Albian sequences (SQ5 and SQ6) are deposited as sub-parallel clinoforms (SF5) (Figs. 6 and 7). A further proof of this is seen in the northern part of our study area because of the serration of gamma-ray log seen in well A1 (Figs. 6a and 7a). The serration of logs is a common occurrence in the shelf margin. These sequences consist of deltaic and fluvio-marine deposits especially in the distal parts which led to a south-easterly distribution of sediments (Gerrard and Smith 1982), causing deposition in an elongated depocentre accompanied by basinward progradation (Dingle et al. 1983). The GR log signature alludes to this fact because of the fining upward Albian-age sequences observed in the northern (A1) and southern section (A2) (Figs. 6 and 7), thus suggesting the influence of fluvial systems on the depositional process. The prograding hummocky (SF2) and divergent (SF6) are an indication of lateral outbuilding and thickening of sedimentary sequences basinward, indicating sediments progradation (Mitchum et al. 1977) in the central part of our study area (Figs and 7). The chaotic (SF4) (South) clinoforms equally suggest soft sediments deformation because of highly variable energy environment accompanying sediments deposition during this period (Fig. 6a–c). The Cenomanian era (SQ4), which

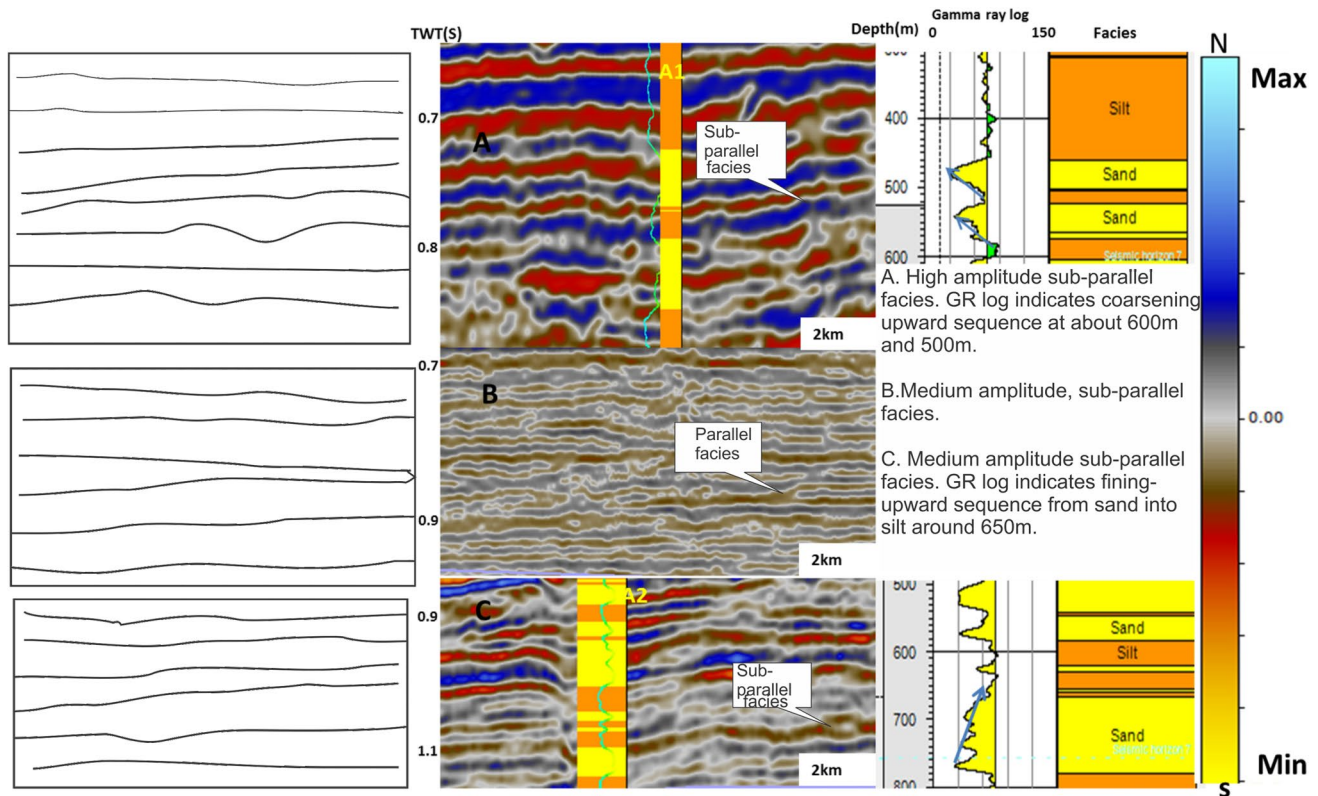


Fig. 10 a–c Campanian/Maastrichtian seismic facies configurations and calibrated gamma-ray log with the lithology interpretations at well positions along the N-S profile. A (North), B (Central) and C

(South). On the left are the conceptual representations of the seismic facies. The horizontal length of each seismic section is 2Km. Note seismic facies mapped in this sequence is Sub-parallel/parallel (SF5)

marked the start of the Upper Cretaceous, is characterised by sub-parallel clinoforms (SF5; Fig. 8), indicating shelfal deposition. The gamma log signature in well A1 is serrated (Fig. 8), suggesting a storm-dominated shelf during this period. The main lithology is siltstone with minor sandstone and shale deposit.

The Turonian sequence (SQ3) was initiated by a marine transgression, followed by a short-span regression, which led to the deposition of localised marine shale and a high accumulation of sediments, respectively (Dingle et al. 1983). This study shows evidence of prograding configuration patterns of hummocky, parallel and chaotic patterns of sedimentation (SF2, SF5 and SF4, respectively, Fig. 9) in this sequence which occurred during the short marine regression. The prograding configurations can be attributed to the short regression which characterised this period (Dingle et al., 1983). The lithologies observed within this sequence are siltstones and sandstone.

The Maastrichtian/Campanian sequence (SQ2) is dominated by sub-parallel and parallel reflectors (SF5, Fig. 10), indicating a subsiding shelf environment, possibly due to the Late Cretaceous margin uplift followed by subsidence during this period, as documented by Guiraud and Bosworth (1997). Delta distributary channels are not unexpected as

the period was characterised by delta progradation due to a regional flooding unconformity (Brown et al., 1996). The evidence of deltaic distributary channels is seen on the GR and lithology log in the northern and the southern part of the study area (Fig. 10a–c). Finally, the Cenozoic unit (SQ1) is characterised by seismic reflection configurations of tangential oblique, hummocky, wavy-parallel and a chaotic patterns, which means that four seismic units (SF1, SF2, SF3 and SF4, respectively) are recognised in this sequence (Fig. 11). The tangential-oblique reflection configuration represents a prodelta shallow slope deposit, which typically contains a terrigenous mix of sand, silt and clay (Badley 1985). The chaotic reflection configuration indicates either soft-sediment deposition or channel-fill deposits, which suggests a variable high-energy environment (Badley 1985). This era was dominated by a drop in the sedimentation rates as the Orange river switched its discharge outlet towards the north of the basin (Dingle and Hendley 1984) because of the cessation of differential crustal subsidence which influenced erosion in the southern part as a result of a topographic barrier (Dingle et al. 1983). The drop in sedimentation rate plus erosion could account for the sediment thickness of less than 300 m for the entire Cenozoic era, as interpreted from the facies log of wells A1 and A2 (Fig. 11).

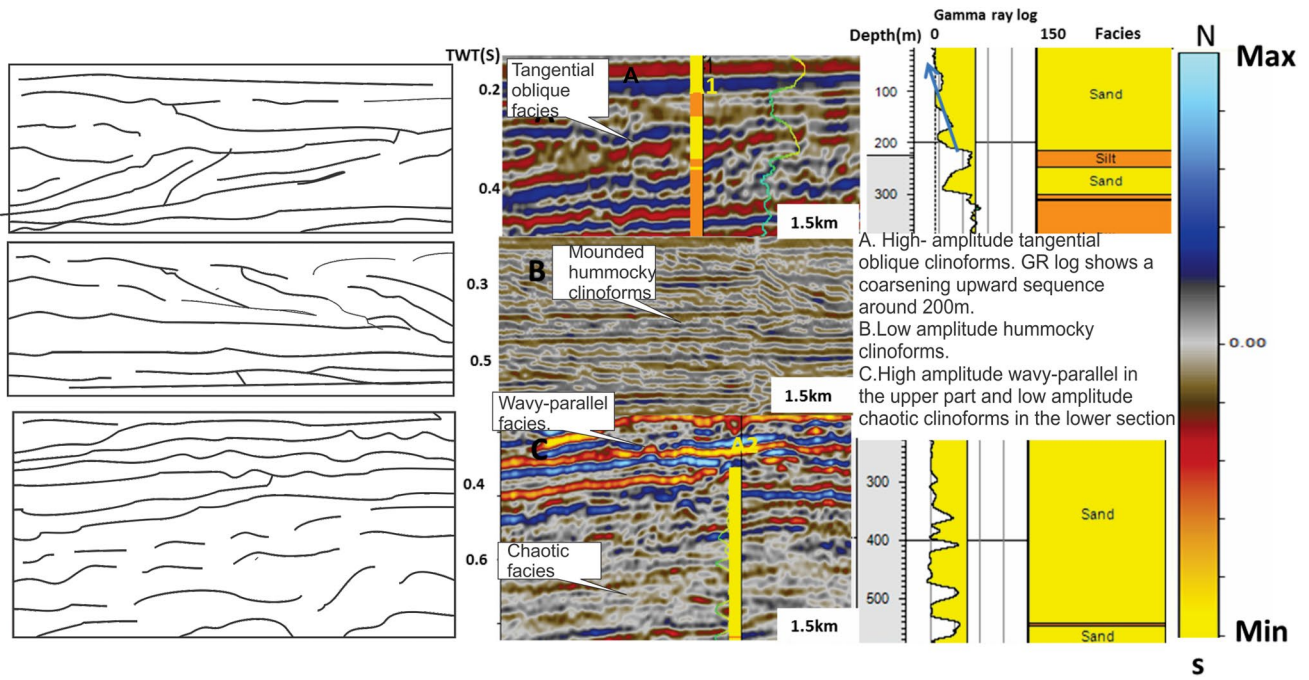


Fig. 11 a–c Cenozoic seismic facies configurations and calibrated gamma-ray log with lithology interpretations at the well positions along the N-S profile. A (North), B (Central) and C (South). On the left are the conceptual representations of the seismic facies. The

horizontal length of each seismic section is 4 km. The seismic facies mapped in this sequence are Tangential oblique (SF1), Hummocky (SF2), Wavy-parallel (SF3) and Chaotic (SF4)

Potential reservoirs

A potential reservoir is identified around 2.2 s and trace 494–285 on L1 within the SQ7 (Barremian-Aptian sequence) (Fig. 12). The sandstone deposit appears enclosed within a

massive shale unit which suggests a likely heterogeneous reservoir situated North of well A1 (Fig. 12). This supports an earlier interpretation suggests that the SQ7 sequence may have been deposited in an incised valley. The distribution of reservoirs expressed as SF4 facies (Chaotic) in an incised

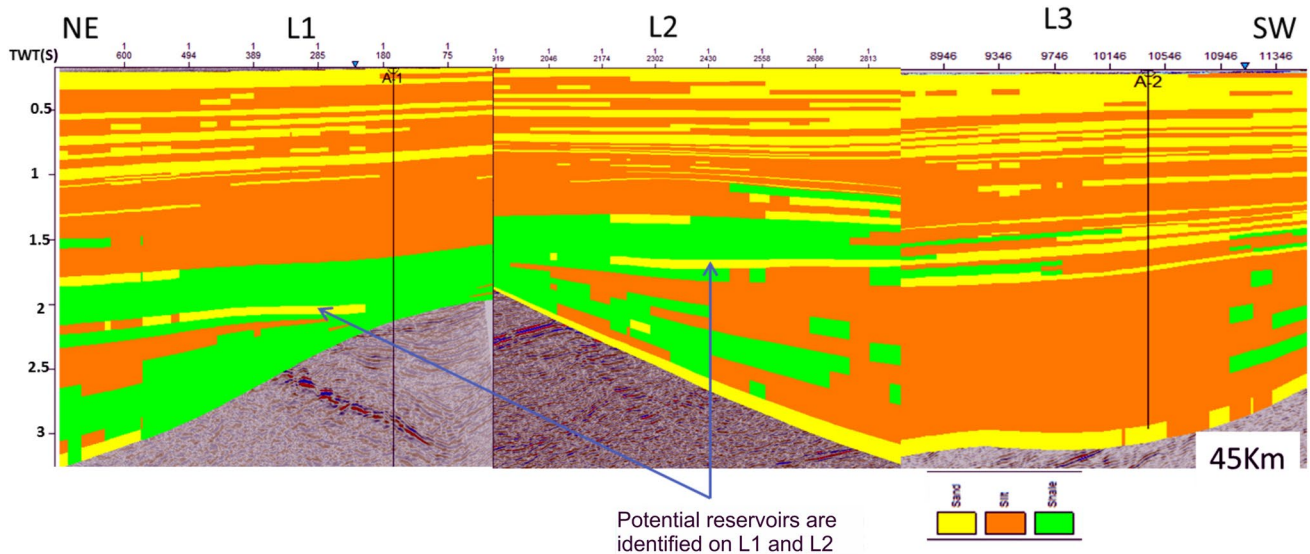


Fig. 12 A cross section of the seismic lines (L1, L2 and L3) and lithofacies integration showing lithology distribution across the study area. Potential reservoirs are identified on the seismic lines L1 and L2 based on the enclosure of the sandstone within the shale units

valley is complex due to a high propensity to accommodate sediments of varying grain sizes, in which highly heterogeneous reservoirs may be present. A laterally extensive sandstone reservoir of Albian age at 2 s TWT and trace 2813 is observed on L2, the geometry as observed here suggests a channel sandstone of Albian age that extends from the Central part towards the South (Fig. 12). The occurrence of Albian fluvial channels as potential reservoirs has been reported in the Orange Basin (Hartwig 2014), thus indicating that the Albian-age reservoirs encountered here may have been of Fluvio-deltaic origin.

Conclusions

This study provides a framework relating seismic and lithofacies for the investigation of passive margin deposits and the delineation of potential hydrocarbon reservoirs in the northern part of the Orange Basin. It also provides insight into palaeo-environmental conditions that accompanied sedimentary evolution in a passive margin setting like the Orange Basin. The main findings of this work are summarised below.

- Six seismic facies were mapped based on the reflection configurations listed in Table 3. They are Tangential-Oblique (SF1), Hummocky (SF2), Wavy-Parallel (SF3), Chaotic (SF4), Sub-parallel/Parallel (SF5) and Divergent (SF6).
- The incised chaotic Incised-Valley Fill of the Barremian-Aptian sequence is evidence of erosion on the coastal plain or shelf in response to a relative sea-level fall that characterised this period, leading to mass transport deposit in the incised valley
- The divergent clinofolds in the Albian sequences point to lateral variations in the rates of deposition, which cause thickening of the individual reflection units inward of the basin (progradation).
- The parallel/sub-parallel clinofolds likely indicate sediment deposition at a uniform rate on a uniformly sub-

siding shelf and are dominant within the Maastrichtian sequence. This could indicate uniform subsidence of the African margin after the late Cretaceous uplift.

- The gamma-ray log signatures at the well positions (A1 and A2) indicate a dominant progradational depositional system from the Late Albian-Turonian. In addition, the serration observed on gamma-ray logs within the Albian and Cenomanian sequences is an indication of sediment deposition on the shelf, which is easily affected by storm and waves, which caused the ‘saw-teeth’-like effect seen on the logs.
- Typically, a potential stratigraphic reservoir is expected to be bounded at the top and bottom by an impermeable lithology, which often is shale or a calcareous siltstone. In this study, the reservoir target is the heterogeneous sandstones unit within the chaotic facies unit (SF4) of the Barremian-Aptian sequence south of well A1 in the northern section (Fig. 12). The sandstone unit is overlain by the Albian shale (potential seal), as seen in proximity to well A1. The deposit is laterally extensive within the 2.2 s TWT and bounded unconformably by shale at the top and bottom as seen close to well A1.
- The fluvio-deltaic sandstone channels of the Albian age close to well A1 which is laterally extensive from L2 towards well A2 could also be a potential reservoir target.

In conclusion, the integration of seismic and lithofacies analyses delineated some reservoir prospects (Albian and Barremian-Aptian), particularly in the northern section of the current study area. Further exploration work, including the acquisition of 3D seismic data and drilling of an exploration well, is recommended in the vicinity of the Barremian-Aptian sandstone deposit, north-east of well A1, to evaluate its thickness, porosity and the net rock volume. These parameters, together with structural or stratigraphic closures, are essential in prospect identification. Figure 13 shows the chronostratigraphic correlation of the two wells used for the study showing the various sequences (SQ1–SQ7) investigated.

Table 3 Summary of seismic facies mapped in the study area

Era	Period	Age (Mya)	Code	Reflection characters/con-figuration	Seismic facies unit	Depositional system	Lithology	Location
Cenozoic	x	65–0	SQ1	Tangential oblique	SF1	Prograding	Sand/siltstone	North
	x	65–0	SQ1	Hummocky	SF2	Prograding	Unknown	Central
	x	65–0	SQ1	Wavy-Parallel	SF3	Aggrading	Sandstone	South
	x	65–0	SQ1	Chaotic	SF4	Aggrading	Sandstone	South
Mesozoic	Maastrichtian	67–65	SQ2	Sub-parallel	SF5	Aggrading	Siltstone/and Sandstone	North
Mesozoic	Maastrichtian	67–65	SQ2	Sub-parallel	SF5		Unknown	Central
Mesozoic	Maastrichtian	67–65	SQ2	Sub-parallel	SF5	Aggrading/retrograding	Siltstone/and Sandstone	South
Mesozoic	Santonian	Eroded	Eroded	Eroded	Eroded	Eroded	Eroded	Eroded
Mesozoic	Coniacian	No-deposition	No-deposition	No-deposition	No-deposition	No-deposition	No-deposition	No-deposition
Mesozoic	Turonian	93–85	SQ3	Sub Parallel/parallel	SF5	Prograding	Siltstone/sandstone	North
	Turonian	93–85	SQ3	Hummocky	SF2	Prograding	Unknown	Central
	Turonian	93–85	SQ3	Chaotic	SF4	Prograding/retrograding	Siltstone/sandstone/Shale	South
Mesozoic	Cenomanian	110–93	SQ4	Chaotic	SF5	Aggrading	Siltstone/sandstone	North
	Cenomanian	110–93	SQ4	Sub-Parallel	SF5	Unknown	Unknown	Central
	Cenomanian	110–93	SQ4	Chaotic	SF5	Retrograding	Siltstone/sandstone	South
Mesozoic	Late Albian	110.5–110	SQ5	Hummocky	SF2	Aggrading	Siltstone/shale	North
	Late Albian	110.5–110	SQ5	Divergent	SF6	Prograding	Unknown	Central
	Late Albian	110.5–110	SQ5	Chaotic	SF4	Aggrading	Siltstone/sandstones	South
Mesozoic	Albian	112–110	SQ6	Sub-parallel	SF5	Retrograding	Siltstone/shale	North
	Albian	112–110	SQ6	Hummocky/divergent	SF2 and SF6	Prograding	Unknown	Central
	Albian	1121–110	SQ6	Chaotic	SF4	Retrograding/Aggrading	Siltstone/Shale	South
Mesozoic	Barremian-Aptian	120–112	SQ7	Chaotic Incised-Valley fill	SF4	Prograding/Retrograding	Sandstone/Shale	North
Mesozoic	Barremian-Aptian	120–112	SQ7	Hummocky	SF2		Unknown	Central
Mesozoic	Barremian-Aptian	120–112	SQ7	Chaotic Incised-Valley fill	SF4	Prograding/Retrograding	Siltstone	South

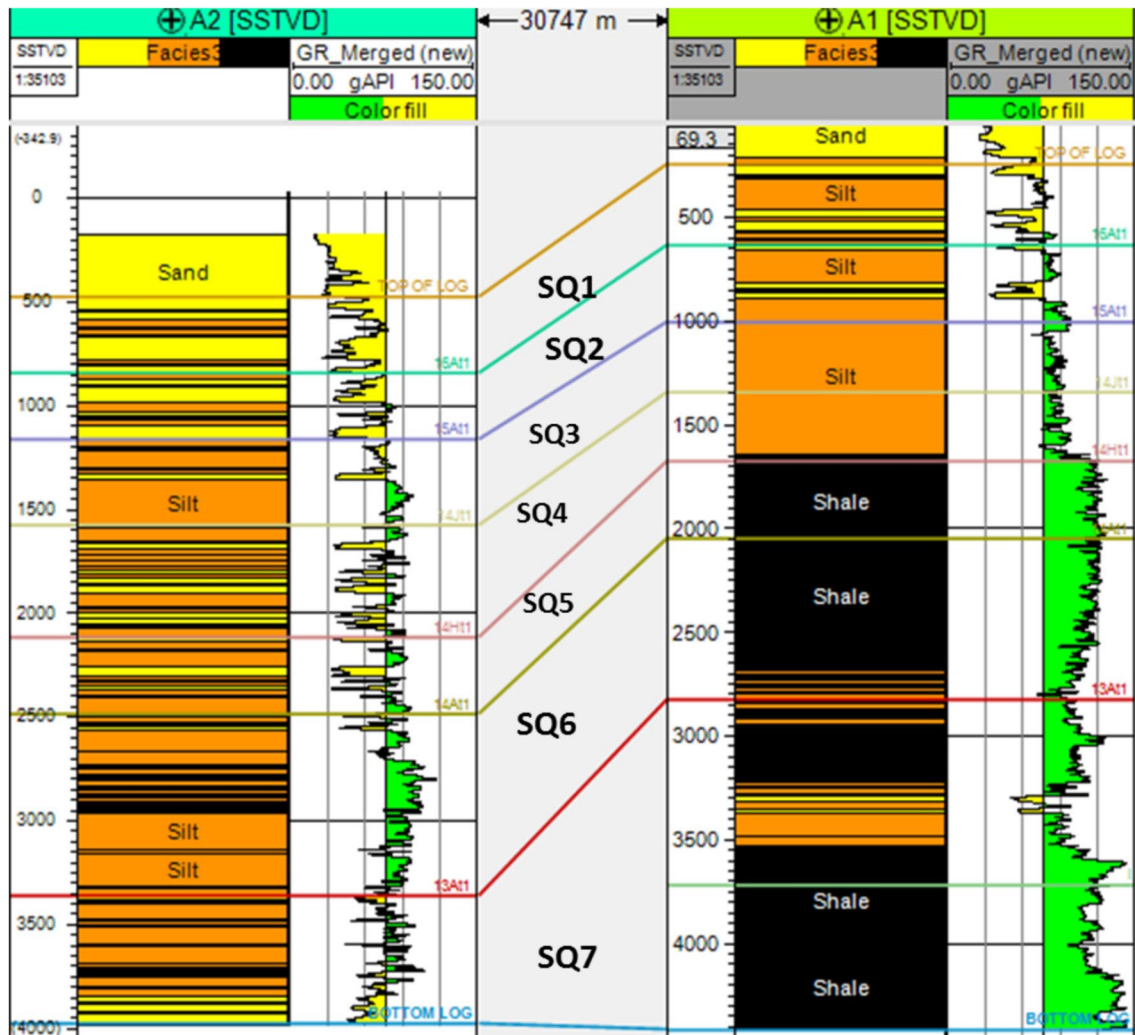


Fig. 13 Chronostratigraphic correlation of wells A2 and A1 (30.7 km apart) showing the major sequences (SQ1-SQ7) mapped within the study area

Acknowledgements Appreciation goes to the National Research Foundation for funding the research. The Petroleum Agency South Africa is appreciated for providing the data used and Schlumberger for providing software support. The School of Geosciences at the University of the Witwatersrand and the Department of Earth Sciences at the University of the Western Cape are equally thanked for their institutional support. RJD acknowledges the support of the Department of Science and Innovation through the South African Research Chairs Initiative (SARChI).

Funding Funding was provided by the Department of Science and Innovation through the Ray Durrheim Research Chair Initiative.

Compliance with ethical standards

Conflict of interest The authors declare that they have no conflict of interest.

Availability of data and material Data are available on request.

Open Access This article is licensed under a Creative Commons Attribution 4.0 International License, which permits use, sharing, adaptation, distribution and reproduction in any medium or format, as long as you give appropriate credit to the original author(s) and the source, provide a link to the Creative Commons licence, and indicate if changes were made. The images or other third party material in this article are included in the article's Creative Commons licence, unless indicated otherwise in a credit line to the material. If material is not included in the article's Creative Commons licence and your intended use is not permitted by statutory regulation or exceeds the permitted use, you will need to obtain permission directly from the copyright holder. To view a copy of this licence, visit <http://creativecommons.org/licenses/by/4.0/>.

References

Badley ME (1985) Practical seismic interpretation. International Human Resources Development Corporation, Boston, p 266

- Bauer K, Neben S, Schreckenberger B, Emmermann R, Hinz K, Fechner N, Gohl K, Schulze A, Trumbull RB, Weber K (2000) Deep structure of the Namibia continental margin as derived from integrated geophysical studies. *J Geophys Res* 25:829–853
- Bradley DC (2008) Passive margins through earth history. *Earth Sci Rev* 91:1–26
- Broad DS, Jungslager EHA, McLachlan IR, Roux J (2007) Offshore Mesozoic Basins. In: Johnson MR, Anhaeusser CR, Thomas RJ (eds) *The Geology of South Africa*. Council for Geoscience, Pretoria, pp 553–565
- Brown, L.F., Brown, L.F. Jr., Benson, J.M., Brink, G.J., Doherty, S., Jollands, A., Jungslager, E.H.A., Keenan, J.H.G., Muntingh, A., And Van Wyk, N.J.S., 1996, Sequence stratigraphy in offshore South Africa divergent basins. An atlas on exploration for Cretaceous low-stand traps by SQUEKOR (Pty) Ltd, American Association Petroleum Geologists Study, In: *Geology* 41, 184
- Catuneanu O, O., (2006) Principles of sequence stratigraphy. Elsevier Radarweg Publishing, AE Amsterdam, pp 42–54
- Cross TA, Lessenger MA, 1988, Seismic stratigraphy: Annual review of earth and planetary sciences, 16, 319–354.
- De Vera J, Granado P, Mcclay K (2010) Structural evolution of the Orange Basin gravity-driven system, offshore Namibia. *J Marine Pet Geol* 27:223–237
- Dingle RV, Hendey QB (1984) Late Mesozoic and tertiary sediment supply to the Eastern Cape Basin (SE Atlantic) and paleo-drainage systems in south-western Africa. *J Marine Geol* 56:13–26
- Dingle RV, Siesser WG, Newton AR (1983) Mesozoic and Tertiary geology of Southern Africa. Balkema, Rotterdam, p 375
- Emery KO, Uchupi E, Phillips J, Bowin C, Mascle J (1975) Continental margin off Western Africa Angola to Sierra Leone. *A Assoc Pet Geol Bullet* 59(12):2209–2265
- Fadipe OA, Carey PF, Akinlua A, Adekola SA (2011) Provenance, diagenesis and reservoir quality of the lower Cretaceous sandstones of the Orange Basin South Africa. *S Africa J Geol* 114:433–448
- Fatti JL, Smith GC, Vail PJ, Strauss PJ, Levitt PR (1994) Detection of gas in sandstone reservoirs using AVO analysis: a 3D seismic case history using the Geostack technique. *J Appl Geophys* 9:1362–1376
- Gerrard I, Smith GC (1982) Post-Paleozoic succession and structure of the south-western African continental margin. In: Watkins JS, Drake CL (eds) *Studies in continental margin geology*. American Association of Petroleum Geologists Memoir, London, pp 49–74
- Gladzenko TP, Skogseid J, Eldhom O (1998) Namibia volcanic margin. *J Marine Geophys Res* 20:313–341
- Gladzenko TP, Hinz K, Eldholm O, Meyer H, Neben S, Skogseid J (1997) South Atlantic volcanic margins. *J Geol Soc London* 154:465–470
- Guiraud R, Bosworth W (1997) Senonian Basin inversion and rejuvenation of rifting in Africa and Arabia; synthesis and implications to plate-scale tectonics. *J Tectonophys* 282:39–82
- Hartwig A (2014) Hydrocarbon migration and leakage dynamics of the Orange Basin, South Africa. *Technischen Universität Berlin, Berlin*, p 256
- Jikell NA (1999) Oil and gas potential of the South African offshore basins. *J Afr Earth Sci GSA* 11, abstracts 33
- Jungslager E (1999) Petroleum habitats of the Atlantic margin of South Africa. In: Cameron NR, Bate RH, Clure VS (eds) *The oil and gas habitats of the South Atlantic*. Geological Society of London Special Publication, London, pp 153–168
- Kuhlmann G, Adams S, Campher C, Van Der Spuy D, Di Primio R, Horsfield B (2010) Passive margin evolution and its controls on natural gas leakage in the southern Orange Basin, block 3/4, offshore South Africa. *J Marine Pet Geol* 27:973–992
- Levell B, Argent J, Dore AG, Fraser S (2009) Passive margins: overview. In: *Petroleum Geology: From Mature Basins to New Frontiers*. Proceedings of the 7th Petroleum Geology Conference, pp 823–830
- Lutgens FK, Tarbuck EJ (2014) *Essentials of Geology*. Pearson's Ltd
- Mann P, Gahagan L, Gordon MB (2003) Tectonic setting of the world's giant oil and gas fields. *A Assoc Pet Geol Tulsa OK Memoirs* 78:15–105
- Mitchum Jr., R.M., Vail, P.R., And Thompson Iii, S., 1977, Seismic stratigraphy and global changes of sea-level. Part 2: the depositional sequence as a basic unit for stratigraphic analysis, In: Payton, C.E. (Ed.), *Seismic Stratigraphy—Applications to Hydrocarbon Exploration* American Association of Petroleum Geologists, Memoir 26, 48–62.
- Petroleum Agency South Africa Report 2006, Petroleum exploration information and opportunities: Petroleum Agency Brochure, 32 p.
- Rebesco M, Mosher D, Piper DJW (2017) Advancements in understanding deep-sea clastic sedimentation processes: a preface. *J Marine Geol* 393:1–3
- Samakinde C, Opuwari M, Van Bever Donker M (2016) The effects of clay diagenesis on petrophysical properties of the lower Cretaceous sandstone reservoirs Orange Basin South Africa. *S African J Geol* 119:187–202
- Sangree JB, Widmier JM (1977) Seismic interpretation of clastic depositional facies. *A Assoc Pet Geol Memoir* 26:165–184
- Sangree JB, Widmier JM (1979) Interpretation of depositional facies from seismic data. *J Geophys* 44:31–60
- Scotchman, I. C., Gilchrist, G., Kuszniir, N. J., Roberts, A. M. and Fletcher, R.2010, The breakup of the South Atlantic Ocean: formation of failed spreading axes and blocks of thinned continental crust in the Santos Basin, Brazil and its consequences for petroleum system development. In: Vining, B. A. & Pickering, S. C. (eds) *Petroleum Geology: From Mature Basins to New Frontiers—Proceedings of the 7th Petroleum Geology Conference*. Geological Society, London, 855–866; doi:<https://doi.org/10.1144/0070855>.
- Vail PR (1987) Seismic stratigraphy interpretation procedure. In: Bally AW (ed) *Atlas of seismic stratigraphy*. American Association of Petroleum Geology Studies in Geology, Tulsa, pp 1–10
- Vining, B.A and Pickering, S. C. 2010 (Eds) *Petroleum geology: from mature basins to new frontiers—proceedings of the 7th petroleum geology conference*, 823–830. Doi: <https://doi.org/10.1144/0070823>.
- Zhu Y, Bhattacharya JP, Li W, Lapen TJ, Jicha BR, Singer BS (2012) Milankovitch-scale sequence stratigraphy and stepped forced regressions of the Turonian Ferron Notom deltaic complex, south-central Utah, USA. *J Sediment Res* 82:723–746

Publisher's Note Springer Nature remains neutral with regard to jurisdictional claims in published maps and institutional affiliations.